J|A|C|S
ARTICLES
Published on Web 11/04/2004

The Complex of a Bivalent Derivative of Galanthamine with *Torpedo* Acetylcholinesterase Displays Drastic Deformation of the Active-Site Gorge: Implications for Structure-Based Drug Design

Harry M. Greenblatt,[†] Catherine Guillou,[§] Daniel Guénard,[§] Anat Argaman,[||] Simone Botti,[||] Bernard Badet,[§] Claude Thal,[§] Israel Silman,[‡] and Joel L. Sussman*[,†]

Contribution from the Departments of Structural Biology and Neurobiology, Weizmann Institute of Science, Rehovot 76100, Israel, Institut de Chimie des Substances Naturelles, C.N.R.S., Avenue de la Terrasse F-91190 Gif-sur-Yvette CEDEX, France, and BioStrX Ltd., 2a Katzir Street, Ramat Gan, 52656, Israel

Received June 9, 2004; E-mail: joel.sussman@weizmann.ac.il

Abstract: Bifunctional derivatives of the alkaloid galanthamine, designed to interact with both the active site of the enzyme acetylcholinesterase (AChE) and its peripheral cation binding site, have been assayed with *Torpedo californica* AChE (*Tc*AChE), and the three-dimensional structures of their complexes with the enzyme have been solved by X-ray crystallography. Differences were noted between the IC_{50} values obtained for *Tc*AChE and those for *Electrophorus electricus* AChE. These differences are ascribed to sequence differences in one or two residues lining the active-site gorge of the enzyme. The binding of one of the inhibitors disrupts the native conformation of one wall of the gorge, formed by the loop Trp279−Phe290. It is proposed that flexibility of this loop may permit the binding of inhibitors such as galanthamine, which are too bulky to penetrate the narrow neck of the gorge formed by Tyr121 and Phe330 as seen in the crystal structure.

Introduction

Alzheimer's disease (AD) is a progressive neurodegenerative disorder of the central nervous system (CNS), resulting in dementia that is characterized by profound memory impairments, emotional disturbance, and personality changes. Synaptic dysfunction or loss appears to be a critical element in producing the symptoms of dementia. Neurochemical and neuroanatomical studies suggest that cholinergic neurons in the neocortex and hippocampus are those predominantly affected in AD. This led to the cholinergic hypothesis, which associates AD symptoms with cholinergic deficiency.[1−3] Symptomatic treatment for AD has thus focused, so far, upon augmenting cholinergic neurotransmission. Precursors of acetylcholine (ACh), such as lecithin and choline, were ineffective in increasing central cholinergic activity,[4−6] and attempts to increase activation of postsynaptic cholinergic receptors by use of cholinergic agonists produced unacceptable adverse effects.[7−10] Currently, the most effective way of augmenting the reduced levels of ACh in afflicted individuals is by use of inhibitors of acetylcholinesterase (AChE), the enzyme responsible for degrading ACh in the synaptic cleft. The synthetic compounds E2020 (Aricept)[11,12] and rivastigmine (Exelon)[13,14] are the two principal drugs used currently for management of AD. Huperzine A (HupA),[15] an alkaloid derived from a moss employed in traditional Chinese medicine, which is also an AChE inhibitor,[16,17] is being used to treat AD in China. Galanthamine **1** (GAL; Reminyl), is an

[†] Department of Structural Biology, Weizmann Institute of Science.
[‡] Department of Neurobiology, Weizmann Institute of Science.
[§] ICSN, CNRS.
[||] BioStrX.

(1) Dunnett, S. B.; Fibiger, H. C. *Prog. Brain Res.* **1993**, *98*, 413−420.
(2) Weinstock, M. *J. Neural Transm. Suppl.* **1997**, *49*, 93−102.
(3) Bartus, R. T.; Dean, R. L.; Beer, B.; Lippa, A. S. **1982**, *217*, 408−414.
(4) Etienne, P.; Dastoor, D.; Gauthier, S.; Ludwick, R.; Collier, B. *Neurology* **1981**, *31*, 1552−1554.
(5) Thal, L. J.; Rosen, W.; Sharpless, N. S.; Crystal, H. *Neurobiol. Aging* **1981**, *2*, 205−208.
(6) Heyman, A.; Schmechel, D.; Wilkinson, W.; Rogers, H.; Krishnan, R.; Holloway, D.; Schultz, K.; Gwyther, L.; Peoples, R.; Utley, C.; Haynes, C. *J. Neural Transm. Suppl.* **1987**, *24*, 279−286.
(7) Gray, J. A.; Enz, A.; Spiegel, R. *Trends Pharmacol. Sci.* **1989**, 85−88.
(8) Harbaugh, R. E.; Roberts, D. W.; Coombs, D. W.; Saunders, R. L.; Reeder, T. M. *Neurosurgery* **1984**, *15*, 514−518.
(9) Harbaugh, R. E.; Reeder, T. M.; Senter, H. J.; Knopman, D. S.; Baskin, D. S.; Pirozzolo, F.; Chui, H. C.; Shetter, A. G.; Bakay, R. A. E.; Leblanc, R.; Watson, R. T.; Dekosky, S. T.; Schmitt, F. A.; Read, S. L.; Johnston, J. T. *J. Neurosurg.* **1989**, *71*, 481−486.
(10) Bodick, N. C.; Offen, W. W.; Levey, A. I.; Cutler, N. R.; Gauthier, S. G.; Satlin, A.; Shannon, H. E.; Tollefson, G. D.; Rasmussen, K.; Bymaster, F. P.; Hurley, D. J.; Potter, W. Z.; Paul, S. M. *Arch. Neurol.* **1997**, *54*, 465−473.
(11) Kawakami, Y.; Inoue, A.; Kawai, T.; Wakita, M.; Sugimoto, H.; Hopfinger, A. J. *Bioorg. Med. Chem. Lett.* **1996**, *4*, 1429−1446.
(12) Kryger, G.; Silman, I.; Sussman, J. L. *Structure* **1999**, *7*, 297−307.
(13) Weinstock, M.; Razin, M.; Chorev, M.; Enz, A. *J. Neural Transm. Suppl.* **1994**, *43*, 219−225.
(14) Bar-On, P.; Millard, C. B.; Harel, M.; Dvir, H.; Enz, A.; Sussman, J. L.; Silman, I. *Biochemistry* **2002**, *41*, 3555−3564.
(15) Raves, M. L.; Harel, M.; Pang, Y.-P.; Silman, I.; Kozikowski, A. P.; Sussman, J. L. *Nat. Struct. Biol.* **1997**, *4*, 57−63.
(16) Wang, Y. E.; Yue, D. X.; Tang, X. C. *Acta Pharmacol. Sin.* **1986**, *7*, 110−113.
(17) Kozikowski, A. P.; Thiels, E.; Tang, X.-C.; Hanin, I. *Adv. Med. Chem.* **1992**, *1*, 175−205.

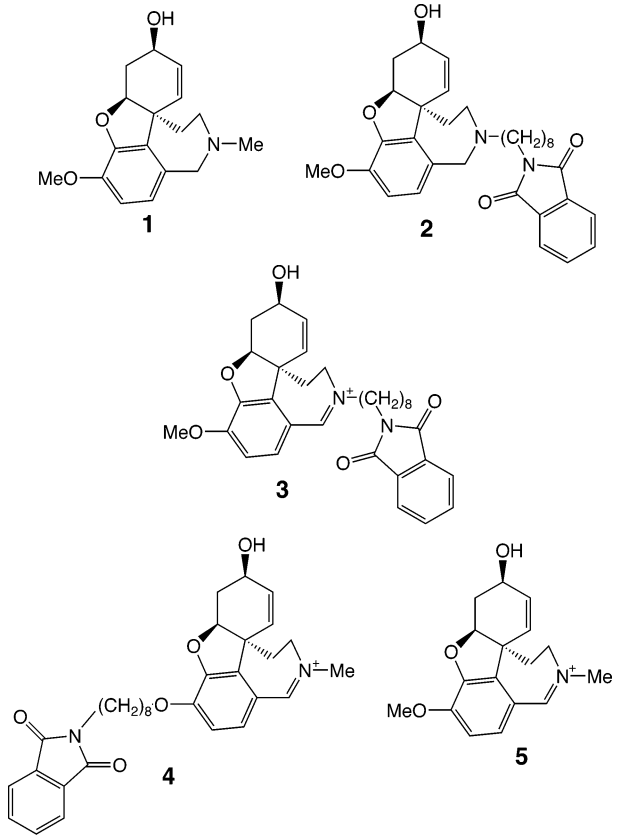

Figure 1. Structures of galanthamine derivatives.

alkaloid found in many members of the *Amaryllidaceae* family, in particular in the common snowdrop (*Galanthus nivalis*). It is also an AChE inhibitor and was recently approved for use in AD treatment. There is also evidence that GAL displays an increased beneficial effect due to its agonist action on nicotinic ACh receptors in the CNS.[18]

In an effort to increase the affinity of GAL for AChE, a series of GAL derivatives was synthesized,[19] aimed at creating bis-acting compounds, that is, compounds which interact with two binding sites on the AChE molecule, thus taking advantage of the "chelate effect".[20] The sites targeted on AChE were the two "anionic" binding sites,[21] the "anionic" subsite of the active site, at the bottom of the active-site gorge, and the "peripheral" anionic site, near the top of the gorge. Inhibition studies showed that derivatives of GAL (or of its iminium salt), in which a phthalimido moiety was attached via an alkyl linker of appropriate length, produced inhibitors with a greater affinity for AChE than that of GAL.[19] In the current study, we describe the crystal structures of complexes of *Torpedo californica* AChE (*Tc*AChE) with compounds **3**, **4**, and **5** (Figure 1). The inhibition constants for inhibition of *Tc*AChE by these three compounds are determined and compared with values obtained for *Electrophorus electricus* AChE (*Ee*AChE).

Methods

Inhibitors. Compounds **3**, **4**, and **5** were synthesized as previously described.[19]

Acetylthiocholine iodide (ATC) and 5,5′-dithiobis(2-nitrobenzoic acid) (DTNB) were purchased from Sigma (St. Louis, MO).

Enzymes. *Ee*AChE was purchased from Sigma (reference C-2888).

*Tc*AChE was purified from electric organ tissue of *T. californica* as described.[15,22]

Enzymatic Assays. Inhibition of AChE activity was determined by the spectroscopic method of Ellman et al.,[23] using acetylthiocholine iodide as substrate, in 96-well microtiter plates.[24] All solutions were brought to room temperature prior to use. Aliquots of 640 μL of 10 mM DTNB in 0.1 M sodium phosphate, pH 8.0, 19.2 μL of the same buffer, and 13 μL of a solution of AChE (100U/mL) in water were added to each well, followed by 2 μL of an aqueous solution of the inhibitor. The reaction was initiated by adding 20 μL of acetylthiocholine iodide (7.5 mM) to each well, and followed by monitoring the appearance of the thiolate dianion produced by reduction of DTNB at 412 nm for 120 s at 25 °C in a Molecular Devices Spectra Max 384 Plus plate reader. Each inhibitor was evaluated at several concentrations in the range from 10^{-9} to 2×10^{-5} M. Percentage inhibition was calculated relative to a control sample, and IC_{50} values displayed represent the mean $\pm$ standard deviation for triplicate assays.

Crystallographic Analysis. Compounds **3** and **5** were dissolved in 25 mM NaCl/40% PEG 200/100mM MES, pH 5.8, both at a concentration of 10 mM. Trigonal *Tc*AChE crystals[25] were transferred to a 6 μL drop of the soaking solution for 1 day, after which the drops were sucked into capillaries and kept at 4 °C overnight and during travel to the synchrotron. Thus, total exposure time to the inhibitor solutions was ~3 days. Data collection was carried out at the ESRF, Grenoble, France, on beam-line ID-14-2, using an ADSC Quantum 4 detector. For data collection, the crystals were transferred to oil, mounted in nylon loops, and flash-cooled in the cryo-stream (100 K). Optimal data collection protocol was determined with STRATEGY.[26] Data collection parameters are presented in Table 1. Data were processed using DENZO and SCALEPACK.[27] Starting structures were based on native *Tc*AChE (PDB code: 2ace).[15] CNSsolve[28] was used for all aspects of the refinement. The initial step involved rigid-body refinement both to check the handedness of the data and to adjust the model for changes in unit-cell constants. Using difference electron density maps ($F_o - F_c$) from the rigid body refinement, we fitted the inhibitor and some carbohydrate side-chains for both structures, and one round of simulated-annealing torsion-angle refinement[29] was carried out. Subsequent rounds of refinement used positional minimization (five rounds for **3**, four rounds for **5**), during which water molecules were added, and small changes were made to the structure. Peak searches for water molecules were not exhaustive, but particular attention was paid to the region of the active site. During the first round of peak searching in the complex with **5**, a solvent peak in contact with the side-chains of Asp326 and Asp392 and four other solvent ligands (square pyramid) was fit as a Mg^{2+} ion. Refined ligand distances are between 2.0 and 2.2 Å. Final refinement parameters are presented in Table 2.

(18) Santos, M. D.; Alkondon, M.; Pereira, E. F.; Aracava, Y.; Eisenberg, H. M.; Maelicke, A.; Albuquerque, E. X. *Mol. Pharmacol.* **2002**, *61*, 1222−1234.
(19) Mary, A.; Renko, D. Z.; Guillou, C.; Thal, C. *Bioorg. Med. Chem.* **1998**, *6*, 1835−1850.
(20) Jencks, W. P. *Adv. Enzymol. Relat. Areas Mol. Biol.* **1975**, *43*, 219−410.
(21) Harel, M.; Schalk, I.; Ehret-Sabatier, L.; Bouet, F.; Goeldner, M.; Hirth, C.; Axelsen, P.; Silman, I.; Sussman, J. L. *Proc. Natl. Acad. Sci. U.S.A.* **1993**, *90*, 9031−9035.
(22) Sussman, J. L.; Harel, M.; Frolow, F.; Varon, L.; Toker, L.; Futerman, A. H.; Silman, I. *J. Mol. Biol.* **1988**, *203*, 821−823.
(23) Ellman, G. L.; Courtney, K. D.; Andres, V.; Featherstone, R. M. *Biochem. Pharmacol.* **1961**, *7*, 88−95.
(24) Doctor, B. P.; Toker, L.; Roth, E.; Silman, I. *Anal. Biochem.* **1987**, *166*, 399.
(25) Sussman, J. L.; Harel, M.; Frolow, F.; Oefner, C.; Goldman, A.; Toker, L.; Silman, I. *Science* **1991**, *253*, 872−879.
(26) Ravelli, R. B. G.; Sweet, R. M.; Skinner, J. M.; Duisenberg, A. J. M.; Kroon, J. *J. Appl. Crystallogr.* **1997**, *30*, 551−554.
(27) Otwinowski, Z.; Minor, W. *Methods Enzymol.* **1997**, *276*, 307−326.
(28) Brunger, A. T.; Adams, P. D.; Clore, G. M.; DeLano, W. L.; Gros, P.; Grosse-Kunstleve, R. W.; Jiang, J. S.; Kuszewski, J.; Nilges, M.; Pannu, N. S.; Read, R. J.; Rice, L. M.; Simonson, T.; Warren, G. L. *Acta Crystallogr., Sect. D: Biol. Crystallogr.* **1998**, *54* (Pt 5), 905−921.
(29) Brunger, A. T.; Adams, P. D.; Rice, L. M. *Prog. Biophys. Mol. Biol.* **1999**, *72*, 135−155.

Table 1. Data Collection Parameters and Processing Statistics

	5	**3**	**4**	native orthorhombic
space group	$P3_121$	$P3_121$	$P2_12_12_1$	$P2_12_12_1$
oscillation angle, exposure time	0.5°, 7 s	0.5°, 5 s	0.5°, 7 min	0.5°, 10 min
total number of frames	70	130	170	195
total number of reflections (rejects)	230 339 (133)	369 491 (931)	652 677 (24)	591 307 (6)
resolution range	40−2.05 Å	40−2.15 Å	35−2.30 Å	40−2.4 Å
number of unique reflections	61 443	52 750	63 928	55 093
overall redundancy	2.1	3.7	3.2	2.5
overall completeness	97.8%	98.9%	98.4%	94.3%
completeness in highest resolution shell	96.5%	100%	98.9%	88.3%
overall R_{merge}	5.2%	6.6%	7.0%	5.7%
R_{merge} in highest resolution shell	30.0% (2.12−2.05 Å)	20.7% (2.23−2.15 Å)	49.8% (2.38−2.3 Å)	27.3% (2.49−2.4 Å)

Table 2. Refinement Results

	5	**3**	native orthorhombic	**4**
resolution range	40.0−2.05 Å	40.0−2.15 Å	40.0−2.40 Å	34.0−2.30 Å
number of protein atoms	4172	4219	4165(A) + 4204(B)	4120(A) + 4122(B)
solvent (water)	245	309	252 (A+B)	114 (A+B)
carbohydrate atoms	28	56	56 (A+B)	56 (A+B)
inhibitor atoms	21	38		21 + 21
R_{work}	19.8%	18.5%	20.4%	23.6%
R_{free} (5% of reflections)	23.2%	21.9%	24.7%	28.3%
rms bond deviations	0.020 Å	0.022 Å	0.015 Å	0.016 Å
rms angle deviations	1.9°	2.0°	1.6°	1.8°
PDB accession code	1W6R	1W4L	1W75	1W76

Compound **4** was dissolved in 25 mM NaCl/40% PEG 200/100 mM MES, pH 5.8, at a final concentration of 2 mM. Attempts to obtain a complex between **4** and *Tc*AChE by soaking trigonal crystals in the inhibitor solution failed, due to a marked degradation in diffraction quality, even when the soaking time was reduced to a few hours. Consequently, orthorhombic crystals of *Tc*AChE, which grow spontaneously in the same drop with the seeded trigonal crystals, were soaked in a 6 μL drop of the same soaking solution for 19 h at 4 °C. A crystal was then transferred to cryoprotectant oil (Hampton Research), mounted on a nylon loop, and flash-cooled in an Oxford Cryosystems Cryostream running at 120 K. Data collection was carried out "in-house", using a Rigaku RU-H3R rotating anode generator running at 50 kV/90 mA with Osmic Confocal Blue optics. Diffraction images were recorded with a Rigaku R-AXIS-IV^{++} detector (100μ mode). The program STRATEGY[26] was used to identify the optimal data collection protocol, and DENZO and SCALEPACK[27] were used to integrate and scale the data (Table 1). The starting model was taken from previous examples of the orthorhombic form,[30,31] which has a noncrystallographic twofold axis relating the subunits of the dimer. Rigid-body refinement[28] was used to orient each molecule in the asymmetric unit to obtain a more accurate matrix for defining the dimer in subsequent refinement steps. Initial electron density maps clearly showed the GAL moiety of **4** bound in the active site of the enzyme, with electron density continuing toward the position of the side-chain of Phe288. Negative electron density (−4σ) around some of the main-chain atoms of Arg289, Phe288, Phe284, and Val281 indicated movement of these residues from their native conformations. For the subsequent round of simulated annealing,[29] residues 282−290, inclusive, were removed from the model. Strict noncrystallographic symmetry (NCS) was imposed. A difference map showed very poor density for most of the residues in the loop (Figure 2). After a further simulated annealing run, followed by a round of standard minimization, residues Leu282, Pro283, and Phe290, the GAL substructure of **4**, 34 water molecules, and one carbohydrate residue were added. At this point, concern arose that differences in the interaction of the inhibitor with the two molecules in the asymmetric unit might be masked by the use of strict NCS. Tests conducted with restrained NCS and without any NCS showed a reduction in the free *R*-factor in both cases. Consequently, a round of simulated annealing was run without NCS, using three different initial velocities, yielding three structures. A difference map generated from the average amplitudes of these three structures failed to reveal any clear density for the missing residues from 284 to 288, but broken density was visible for Arg289 in its native conformation, with no improvement over the initial map shown in Figure 2. Nor was any density visible for seven carbons of the eight-carbon linker or for the phthalimide group of **4**. The addition of 47 water molecules, followed by a further round of simulated annealing (1 initial velocity), did not improve the maps of the missing regions. Final refinement results are presented in Table 2.

To provide a model of the native orthorhombic form refined under conditions similar to those from the complex with **4**, data were collected

(30) Raves, M. Structure−function studies on acetylcholinesterase in space and time. Ph.D. Thesis, Weizmann Institute of Science, Rehovot, Israel, 1998.
(31) Greenblatt, H. M.; Silman, I.; Sussman, J. L., unpublished results.

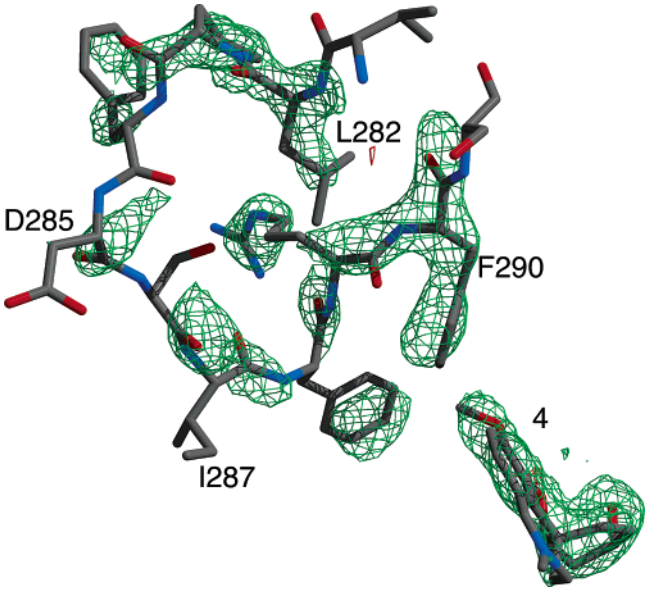

Figure 2. Difference electron density of the region of the Val281−Ser291 loop in the complex of *Tc*AChE with **4**, after simulated annealing in which residues Leu282−Phe290 were omitted. The model of the missing residues is that of the native protein. The map is contoured at 3σ and was made using Xfit[36] and Raster3d.[37]

from an orthorhombic crystal grown during trials of tungsten-cluster effectors.[32] Although no apparent complexes between the tungsten clusters and the protein were visible, the crystals provided higher quality data than those obtained previously from orthorhombic crystals. [31] *Tc*AChE (in 100 mM NaCl/0.01% NaN_3/1 mM MES, pH 6.5) was mixed 1:1 with solubilized $Li_5[PW_{11}O_{39}RhCH_2COOH]$;[33] a 3 μL aliquot was mixed with 3 μL of precipitant solution (40% PEG 200/0.5 M MES, pH 5.8). The protein/precipitant drop was suspended over a well containing 1 mL of 36% PEG 200/0.5 M MES, pH 5.8. Large, well-formed orthorhombic plates appeared after 4 days. A crystal was harvested with a nylon loop and transferred to oil, and the excess solvent was removed. The crystal was then mounted in a nylon loop and flash-cooled in an Oxford Cryosystems cryostream (120 K), mounted on an RU-H3R rotating anode (50 KV, 90 mA). An initial diffraction image (RAXIS-IV^{++}) was processed with DENZO and STRATEGY to determine the optimal data collection strategy. Data collection statistics are summarized in Table 1. Rigid body refinement was used to adjust each molecule in the asymmetric unit independently, followed by individual atom refinement (all in REFMAC5).[34] No NCS was used. Peak searches after each round of refinement revealed parts of the protein chains that needed adjustment and allowed the placement of water molecules. Stringent criteria were used for the assignment of water molecules; thus, long strings of density, which may correspond to parts of PEG 200 molecules, were not fit, nor were peaks with no obvious hydrogen bond donors/acceptors within 4.0 Å. The rms deviation between the two molecules in the asymmetric unit was 0.21 Å for the main-chain atoms (N, C^{α}, and C), and 0.4 Å for all atoms.[35] Final refinement results are listed in Table 2.

Table 3. IC_{50} Values for Inhibition of *Ee*AChE and *Tc*AChE by GAL and Its Derivatives

enzyme	compound	$IC_{50} \pm$ SD nM	$IC_{50}/IC_{50galanthamine}$
	GAL	614 ± 47	1
	2	72 ± 5	0.11
*Ee*AChE	3	11 ± 1	0.02
	4	203 ± 28	0.3
	5	266 ± 32	0.4
	GAL	418 ± 18	1
	2	38 ± 2	0.09
*Tc*AChE	3	4 ± 0.6	0.010
	4	499 ± 98	1.2
	5	702 ± 90	1.7

Results

Kinetic Studies. The *N*-phthalimido compound, **3**, is the most potent inhibitor for both *Ee*AChE and *Tc*AChE, with marked preference for *Tc*AChE (Table 3). Conversely, taking $IC_{50-galanthamine}$ as an internal reference for both enzymes, the $IC_{50}/IC_{50-galanthamine}$ values indicate that both **4** and **5** are better inhibitors of *Ee*AChE than of *Tc*AChE, with *Tc*AChE/*Ee*AChE IC_{50} ratios of ~4. This difference may be due to the presence of a tyrosine residue in *Ee*AChE (Tyr355) at the position equivalent to Phe330 in *Tc*AChE. The ability of the O^{η} of the tyrosine to interact with the iminium function present in **5** may account for the increased affinity for the eel enzyme. More detailed comparisons between *Ee*AChE and *Tc*AChE are not possible at this time, due to the lack of any high-resolution data for the former enzyme.[38,39]

Structures of *Tc*AChE Complexes. Compound 5. The overall binding mode of the GAL scaffold of **5**, in its complex with *Tc*AChE, as shown in Figure 3, is essentially identical to that reported for GAL itself.[40,41] One noteworthy difference is the change in the position of the side-chain of Phe330 in the complex with **5**, relative to that with GAL. Because **5** bears a quaternary nitrogen atom, interactions involving a bound PEG hydroxyl group or a water molecule, and the flat face of the benzyl ring of Phe330, are precluded. Consequently, the side-chain of Phe330 moves to cover the dihydroazepine ring of **5**. These differences are reflected in the slightly decreased affinity of **5**, relative to GAL itself, for *Tc*AChE (Table 3).

Compound 3. As for **5**, the binding mode of the GAL-like moiety of **3** is essentially identical to that of GAL (Figure 3). The attached alkyl chain snakes up the gorge, and the phthalimido group stacks against the surface of the indole group of Trp279. The increased affinity of **3** presumably results from the increased surface area of contact between the inhibitor and the enzyme, particularly around Trp279. It is not apparent why **3**, the imine derivative of GAL, binds better than the native GAL derivative, **2**, especially because the imine modification alone, in **5**, results in a larger IC_{50}. The enhanced affinity of **3**

(32) Weinstein, S.; Jahn, W.; Glotz, C.; Schlunzen, F.; Levin, I.; Janell, D.; Harms, J.; Kolln, I.; Hansen, H. A.; Gluhmann, M.; Bennett, W. S.; Bartels, H.; Bashan, A.; Agmon, I.; Kessler, M.; Pioletti, M.; Avila, H.; Anagnostopoulos, K.; Peretz, M.; Auerbach, T.; Franceschi, F.; Yonath, A. *J. Struct. Biol.* **1999**, *127*, 141−151.
(33) Wei, X. Y.; Dickman, M. H.; Pope, M. T. *J. Am. Chem. Soc.* **1998**, *120*, 10254−10255.
(34) Murshudov, G. N.; Vagin, A. A.; Dodson, E. J. *Acta Crystallogr., Sect. D* **1997**, *53*, 240−255.
(35) Kleywegt, G. J. *LSQMAN*, 010126/7.7.1; Department of Mol. Biol., University of Uppsala: Uppsala, Sweden, 2001.
(36) McRee, D. E. *J. Struct. Biol.* **1999**, *125*, 156−165.
(37) Merritt, E. A.; Bacon, D. J. *Methods Enzymol.* **1997**, *277*, 505−524.
(38) Raves, M.; Giles, K.; Schrag, J. D.; Schmid, M. F.; Phillips, G. N.; Chiu, W.; Howard, A. J.; Silman, I.; Sussman, J. L. Quaternary structure of tetrameric acetylcholinesterase. In *Structure and Function of Cholinesterases and Related Proteins*; Doctor, B. P., Taylor, P., Quinn, D. M., Rotundo, R. L., Gentry, M. K., Eds.; Plenum: New York, 1998; pp 351−356.
(39) Bourne, Y.; Grassi, J.; Bougis, P. E.; Marchot, P. *J. Biol. Chem.* **1999**, *274*, 30370−30376.
(40) Greenblatt, H. M.; Kryger, G.; Lewis, T.; Silman, I.; Sussman, J. *FEBS Lett.* **1999**, *463*, 321−326.
(41) Bartolucci, C.; Perola, E.; Pilger, C.; Fels, G.; Lamba, D. *Proteins* **2001**, *42*, 182−191.

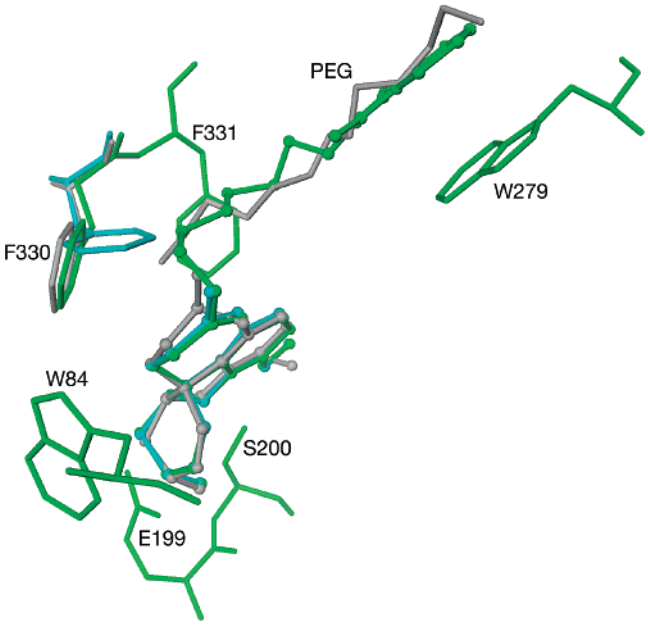

Figure 3. Overlap of the structures of the complexes of *Tc*AChE with compounds **1**, **3**, and **5**. Inhibitors are rendered as ball-and-stick models, while protein and PEG atoms are rendered as sticks. The complex with **1** is colored gray, that with **3** is depicted in green, and that with **5** is in cyan. Protein side-chains are shown only for the complex with **3**, except for Phe330, for which the orientation is different in the complex with **5**. The PEG molecule was observed in the complex with **1**. The picture was made using DINO.[42]

Table 4. Deviation from Mean Main-Chain *B*-Factors ($\langle B_{mc} \rangle$) in the Complex of **4** with *Tc*AChE

	native orthorhombic form		complex with **4**	
	chain A $\langle B_{mc} \rangle = 32$	chain B $\langle B_{mc} \rangle = 33$	chain A $\langle B_{mc} \rangle = 42$	chain B $\langle B_{mc} \rangle = 43$
Trp279	−11%	3.4%	26%	33%
Asn280	−15%	2%	31%	39%
Val281	−17%	−2.6%	32%	37%
Leu282	−4.8%	2.0%	41%	46%
Pro283	4.8%	11%	44%	52%
Phe284	9.7%	17%		
Asp285	5.3%	17%		
Ser286	−6.4%	4.4%		
Ile287	−16%	−9.0%		
Phe288	−20%	−18%		
Arg289	−21%	−18%		
Phe290	−19%	−16%	1%	7%
Ser291	−22%	−16%	−3%	10%

relative to **2** may be due to a decrease in conformational flexibility associated with the double bond of the dihydroazepine ring.

Compound 4. Despite the presence of a large group on the *O*-methyl portion of the GAL-like substructure, **4** binds in the same basic orientation as GAL. To accommodate the linker group in the acetyl-binding pocket, large movements of the loop containing Phe288 occur. Residues 285−288, as well as the eight-carbon linker and the phthalimide moiety, do not appear to have a single stable conformation, as evidenced by the lack of clear electron density for their atoms. Those residues in the 279−289 loop that are visible have elevated *B*-factors relative to the native structure (see Table 4). The increased mobility of the loop can be visualized as an aperture in the wall of the gorge, as shown in Figure 4, which connects the acyl-binding pocket with the exterior. The phthalimide, together with the distal

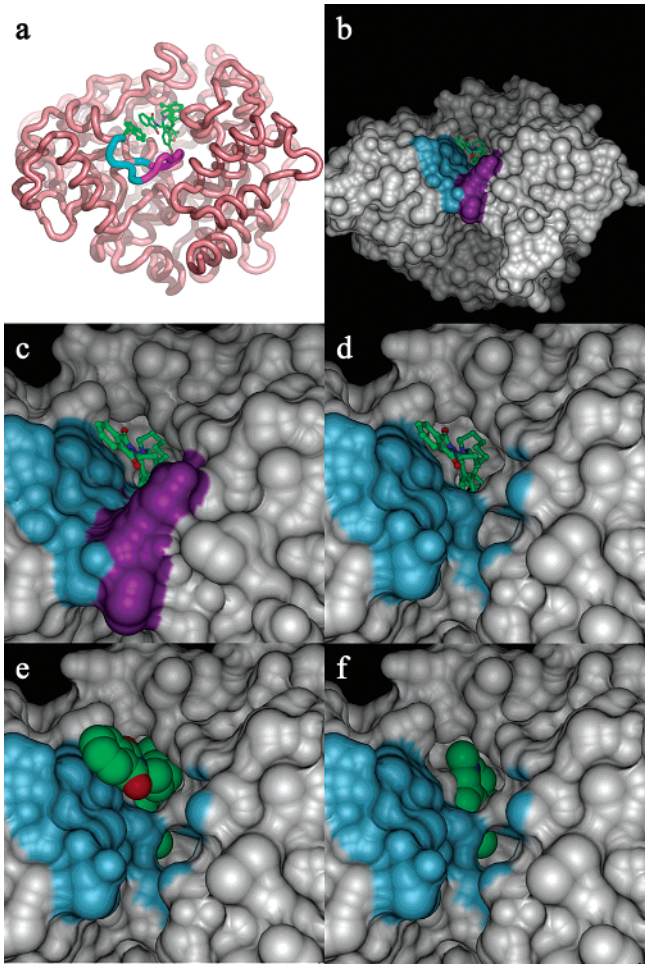

Figure 4. Sequence of pictures showing the region affected by binding of **4** to *Tc*AChE. (a) C^{α} trace of the complex of *Tc*AChE with **3**. The inhibitor is rendered as a stick model, while the side-chains of Trp279 and Trp84 are shown as ball-and-stick models. The section of the polypeptide chain from Trp279 to Phe290 is colored light blue, while the subsection from Phe284 to Arg289 is colored magenta. (b) Same view as in (a), but showing the molecular surface. Sections of the surface formed by the Trp279−Phe290 loop are colored as in (a). (c) Close-up of the view shown in (b). (d) Same view as in (c), but showing the surface of the complex of *Tc*AChE with **4**; compound **3**, in ball-and-stick format, is modeled into the structure for reference. (e) Same view as in (d), but with **3** rendered in CPK. The *O*-methyl group of the GAL substructure of **3**, bound in the acyl pocket, is partially visible. (f) Same view as in (e), but showing compound **4**, rendered as a CPK model, bound in the active site, as seen in the crystal structure. The *O*-methyl group, to which the linker and phthalimide groups are attached, is partially visible through the hole in the wall of the acyl pocket. The pictures were made using PyMOL, DINO, and POV-ray.

carbons of the linker, presumably protrude through this opening into the solvent.

The difference in behavior between the trigonal and orthorhombic crystals of *Tc*AChE with respect to tolerance of the binding of **4** can be explained by comparing the packing of the protein molecules in the two crystal forms. Figure 5 shows that in the trigonal form, the Trp279−Phe290 loop, whose surface is shown in magenta, makes close contacts with a symmetry-related AChE molecule which largely occludes the entrance to the active-site gorge. Permanent and large rearrangements of this loop would, therefore, be expected to disrupt crystal packing. In the orthorhombic crystals, the symmetry-related molecule does not interact closely with the Trp279−Phe290 loop;

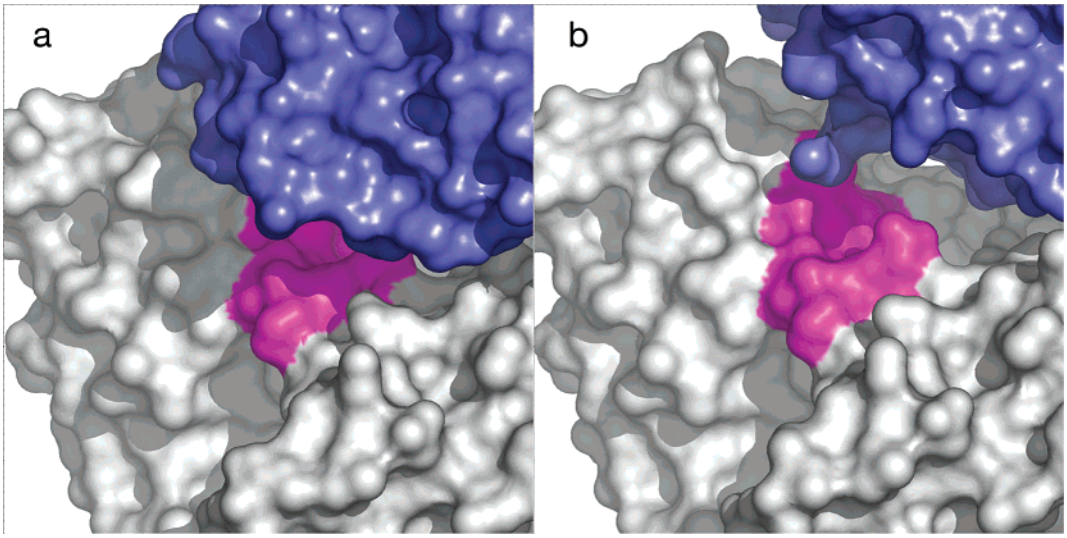

Figure 5. Comparison of symmetry-related contacts in the trigonal and orthorhombic crystal forms of *Tc*AChE. (a) Native trigonal form; (b) native orthorhombic form. In both, the reference molecule is shown with a white/gray surface, and the symmetry-related molecule is shown with a blue surface. The surface of the Trp279−Phe290 loop is colored magenta in the reference molecule. The pictures were made using PyMOL.[43]

consequently, rearrangements of this loop can be tolerated by the crystal lattice.

Discussion

The IC_{50} values displayed in Table 3 show that both of the bifunctional GAL derivatives, **2** and **3**, bind more tightly than GAL itself to *Tc*AChE (>11- and >104-fold, respectively). The enhanced potency of **3**, relative to GAL, is consistent with the crystal structure of the *Tc*AChE/**3** complex, which clearly reveals binding of the GAL moiety within the active site and of the phthalimide moiety to the peripheral anionic site.

While the observed binding modes of **3** and **5** were easily predictable, the binding mode of the GAL substructure of **4** is quite unexpected. In general, structure-based drug design treats the backbone of the protein as a rigid entity. Once the structure of a complex of the protein with a representative ligand has been solved experimentally, it is taken as a valid template, on the basis of which atoms or functional groups can be added to the representative ligand only if free space is available around it within the binding pocket. Obviously, reality is more complex, because protein side-chains may move to accommodate a ligand,[12,21] and in some cases there may even be limited movement of the polypeptide backbone.[44] Moreover, in other cases, bound solvent may define the surface of the binding pocket, rather than the protein itself, and thus limit the space available for addition of substituents.[15,45] In the present case, structure-based design, using the experimental GAL/*Tc*AChE structure as the template, would predict that **4** could not bind to the active site of AChE, with the same orientation as native GAL, due to the obvious steric hindrance in the acyl binding pocket. Nevertheless, binding in this orientation does occur, as a consequence of the added phthalimide moiety piercing the fabric of the protein, and protruding into the solvent. While these results may be an extreme example, they do emphasize the limitations in reliance on structure-based drug design, which considers the protein as a rigid template. Although some programs use molecular dynamics or flexible docking to allow for movement of the protein, we are not aware of any approach that could take into account such drastic tearing of the protein fabric.

The 3D structure of AChE, in which access to the active site is via a long and narrow gorge,[25] raises cogent questions concerning traffic of substrates, products, and solvent to and from the active site.[46] At its narrowest point, the diameter of the gorge is considerably smaller than the diameter of the quaternary group of choline, and there is a steep electrostatic potential gradient along the gorge axis,[47] which should both assist penetration of the substrate, ACh, and retard the exit of choline. Furthermore, it is not immediately apparent how bulky and rigid reversible inhibitors such as the alkaloids, galanthamine and huperzine A and B, are able to reach the active site, although recent steered molecular dynamics simulations indicate that both entrance and exit of huperzine A can occur along the trajectory of the gorge axis.[48] These issues led to the proposal that one or more alternative routes to the active site might exist, the so-called "back-door" hypothesis.[49,50] This proposal has been the subject of much controversy. Molecular dynamics suggests the existence of one or more transient openings in the wall of the active-site gorge, large enough to permit at least transit of solvent.[51−53] Experimental evidence,

(42) Philippsen, A. *DINO: Visualizing Structural Biology*; 2000.
(43) DeLano, W. L. *The PyMOL Molecular Graphics System*; DeLano Scientific: San Carlos, CA, 2003.
(44) Millard, C. B.; Kryger, G.; Ordentlich, A.; Harel, M.; Raves, M.; Greenblatt, H. M.; Segall, Y.; Barak, D.; Shafferman, A.; Silman, I.; Sussman, J. L. *Biochemistry* **1999**, *38*, 7032−7039.
(45) Koellner, G.; Kryger, G.; Millard, C. B.; Silman, I.; Sussman, J. L.; Steiner, T. *J. Mol. Biol.* **2000**, *296*, 713−735.
(46) Botti, S. A.; Felder, C.; Lifson, S.; Sussman, J. L.; Silman, I. *Biophys. J.* **1999**, *77*, 2430−2450.
(47) Felder, C. E.; Botti, S. A.; Lifson, S.; Silman, I.; Sussman, J. L. *J. Mol. Graphics Modell.* **1997**, *15*, 318−327.
(48) Xu, Y. C.; Shen, J. H.; Luo, X. M.; Silman, I.; Sussman, J. L.; Chen, K. X.; Jiang, H. L. *J. Am. Chem. Soc.* **2003**, *125*, 11340−11349.
(49) Ripoll, D. R.; Faerman, C. H.; Axelsen, P.; Silman, I.; Sussman, J. L. *Proc. Natl. Acad. Sci. U.S.A.* **1993**, *90*, 5128−5132.
(50) Axelsen, P. H.; Harel, M.; Silman, I.; Sussman, J. L. *Protein Sci.* **1994**, *3*, 188−197.
(51) Gilson, M. K.; Straatsma, T. P.; McCammon, J. A.; Ripoll, D. R.; Faerman, C. H.; Axelsen, P.; Silman, I.; Sussman, J. L. *Science* **1994**, *263*, 1276−1278.
(52) Wlodek, S. T.; Clark, T. W.; Scott, L. R.; McCammon, J. A. *J. Am. Chem. Soc.* **1997**, *119*, 9513−9522.
(53) Tai, K.; Shen, T. Y.; Borjesson, U.; Philippopoulos, M.; McCammon, J. A. *Biophys. J.* **2001**, *81*, 715−724.

however, has not yet provided clear-cut support for this notion.[54−57] Spectroscopic evidence has, however, been presented for flexibility upon ligand binding of the omega loop (Cys69 to Cys96 in mouse AChE) containing the "anionic-site" tryptophan. A site within this loop was suggested as a possible locus for the "back-door", but it has also been proposed that the observed flexibility may reflect conformational changes associated with the entrance of substrate (or other ligands) along the gorge axis.[58,59]

The *Tc*AChE complex with **4** presented here, which shows that the native conformation of the Trp279−Ser291 loop can be severely disrupted, suggests that additional regions of the gorge can undergo substantial movement, facilitating entry of bulky ligands into the active site. This could also provide an explanation for how the leaving group of the carbamate, in the study of Bartolucci et al.,[56] was able to escape.

Initial evidence that residues in the Trp279−Ser291 loop can adopt alternative conformations to that of the native structure was found in the structure of the conjugate of *Tc*AChE with the nerve agent, diisopropyl phosphorofluoridate (DFP; PDB code 2dfp).[44] In this structure, the isopropyl moiety of the organophosphoryl group, which is covalently attached to the active-site serine, displaces both Phe288 and Phe290 from their native positions, coupled to a significant change in the main-chain conformation in the whole loop. Evidence demonstrating the inherent flexibility of this loop has come from site-directed mutagenesis studies.[60] Mutation of *Tc*AChE Leu282, to either serine or alanine, resulted in a substantial decrease in the enzyme's stability. This was ascribed to a decrease in the conformational stability of the Trp279−Ser291 loop, which contains both the acyl-binding pocket residues and Trp279, a key element of the "peripheral" anionic site.

The portal revealed in the complex of *Tc*AChE with **4** may merely be an artifact of ligand binding. Such a portal, if it did represent a "side-door", would appear to provide an alternate exit for the acetyl group, rather than for choline. Perhaps of greater relevance, our structural data suggest facile rearrangement of the Trp279−Ser291 loop, which may produce a significant increase in the diameter of the gorge, facilitating entry of bulky, rigid inhibitors. This rearrangement may also explain the residual activity of the fasciculin/*Tc*AChE complex,[61] although recent simulations suggest other possible routes for substrate entry.[62] While enlargement of the gorge by such a mechanism may also be relevant to the entry of the substrate ACh during catalysis, simulations have demonstrated smaller-scale changes that allow the entry of quaternary ammonium groups,[63] which might suffice for substrate entry.

Acknowledgment. This study was supported by the European Commission Fifth Framework "Quality of Life and Management of Living Resources" Program under Contract No. QLK3-2000-00650, the Kimmelman Center for Biomolecular Structure and Assembly (Rehovot, Israel), the Benoziyo Center for Neurosciences, U.S. Army Medical and Materiel Command under Contract No. DAMD17-02-1-0675, the Kalman and Ida Wolens Foundation, and the Jean and Jula Goldwurm Memorial Foundation. J.L.S. is the Morton and Gladys Pickman Professor of Structural Biology. The tungsten-cluster compounds were the kind gift of Ada Yonath. We thank Lilly Toker for purification of *Tc*AChE.

JA0466154

(54) Kronman, C.; Ordentlich, A.; Barak, D.; Velan, B.; Shafferman, A. *J. Biol. Chem.* **1994**, *269*, 27819−27822.
(55) Faerman, C.; Ripoll, D.; Bon, S.; LeFeuvre, Y.; Morel, N.; Massoulie, J.; Sussman, J. L.; Silman, I. *FEBS Lett.* **1996**, *386*, 65−71.
(56) Bartolucci, C.; Perola, E.; Cellai, L.; Brufani, M.; Lamba, D. *Biochemistry* **1999**, *38*, 5714−5719.
(57) Simon, S.; Le Goff, A.; Frobert, Y.; Grassi, J.; Massoulie, J. *J. Biol. Chem.* **1999**, *274*, 27740−27746.
(58) Shi, J. X.; Boyd, A. E.; Radic, Z.; Taylor, P. *J. Biol. Chem.* **2001**, *276*, 42196−42204.
(59) Shi, J. X.; Tai, K.; McCammon, J. A.; Taylor, P.; Johnson, D. A. *J. Biol. Chem.* **2003**, *278*, 30905−30911.
(60) Morel, N.; Bon, S.; Greenblatt, H. M.; Van Belle, D.; Wodak, S. J.; Sussman, J. L.; Massoulie, J.; Silman, I. *Mol. Pharmacol.* **1999**, *55*, 982−992.
(61) Radic, Z.; Taylor, P. *J. Biol. Chem.* **2001**, *276*, 4622−4633.
(62) Bui, J. M.; Tai, K.; McCammon, J. A. *J. Am. Chem. Soc.* **2004**, *126*, 7198−205.
(63) Bui, J. M.; Henchman, R. H.; McCammon, J. A. *Biophys. J.* **2003**, *85*, 2267−2272.